



# Fast Reconfiguration Maneuvers of a Micro-satellite Constellation Based on a Hybrid Rocket Engine

Antonio Sannino<sup>1</sup> · Stefano Mungiguerra<sup>1</sup> · Sergio Cassese<sup>1</sup> · Raffaele Savino<sup>1</sup> · Alberto Fedele<sup>2</sup> · Silvia Natalucci<sup>2</sup>

Received: 14 November 2023 / Revised: 8 January 2024 / Accepted: 30 January 2024  
© The Author(s) 2024

## Abstract

In this work, the formation flight of the CubeSat cluster RODiO (Radar for Earth Observation by synthetic aperture Distributed on a cluster of CubeSats equipped with high-technology micro-propellers for new Operative services) with respect to a small satellite in LEO (Low Earth Orbit) has been analyzed. RODiO is an innovative mission concept funded by the Italian Space Agency (ASI) in the context of the Alcor program. The small satellite is equipped with an antenna that allows it to function as a transmitter, whereas RODiO functions as a receiver. The extension of the virtual SAR (Synthetic Aperture Radar) antenna can be achieved by establishing an along-track baseline performing an orbital coplanar maneuver. Another interesting scenario is the possibility to create a cross-track baseline performing an inclination change maneuver. Such formation reconfiguration maneuvers can be achieved in relatively short times only by use of a high-thrust propulsion system, i.e., based on conventional chemical technologies. From the study of maneuvers, it is possible to identify the required  $\Delta V$  (order of magnitude of 10 m/s), which represents an input parameter for the design of propulsion system. Among the different kinds of propulsion systems, a Hybrid Rocket Engine was chosen. Based on the previous experience acquired by Department of Industrial Engineering (University of Naples Federico II), the preliminary design of the thrust chamber for a Hybrid Rocket Engine based on Hydrogen Peroxide (91 wt%) of the 10 N-class could be carried out, whose dimensions meet the compactness requirements of the CubeSat (1.5 U, 2 kg).

**Keywords** Hybrid rocket engine · Hydrogen peroxide · CubeSat formation flying · Orbital maneuvers

## List of Symbols

$\Delta Y_{\text{orbit}}$  Along-track baseline variation per orbit, m  
 $\omega$  Argument of perigee, deg  
 $t_b$  Burning time, s

$\Delta i$  Change in orbital inclination, deg  
 $\Delta V$  Change in velocity, m/s  
 $R_E$  Earth radius, m  
 $\mu$  Earth's planetary gravitational constant,  $\text{km}^3/\text{s}^2$   
 $e$  Eccentricity  
 $\rho_f$  Fuel density,  $\text{kg}/\text{m}^3$   
 $m_f$  Fuel mass flow rate, g/s  
 $L_{\text{conv}}$  Length of convergent, m  
 $L_{\text{div}}$  Length of divergent, m  
 $M$  Mass, kg  
 $i$  Orbital inclination, deg  
 $V_{\text{ci}}$  Orbital velocity of initial circular orbit, km/s  
 $\dot{m}_{\text{ox}}$  Oxidizer mass flow rate, g/s  
 $OF$  Oxidant to fuel ratio  
 $G_{\text{ox}}$  Oxidizer mass flux,  $\text{kg}/(\text{m}^2 \text{ s})$   
 $p$  Periapsis, km  
 $\tau_{\text{ci}}$  Period of the initial circular orbit, s  
 $\tau_e$  Period of elliptical orbit, s  
 $D_p$  Port diameter, mm  
 $L_{\text{post}}$  Post-chamber length, mm  
 $L_{\text{pre}}$  Pre-chamber length, mm

✉ Antonio Sannino  
antonio.sannino2@unina.it

Stefano Mungiguerra  
stefano.mungiguerra@unina.it

Sergio Cassese  
sergio.cassese@unina.it

Raffaele Savino  
raffaele.savino@unina.it

Alberto Fedele  
alberto.fedele@asi.it

Silvia Natalucci  
silvia.natalucci@asi.it

<sup>1</sup> Department of Industrial Engineering, University of Naples Federico II, 80 Piazzale Tecchio, 80125 Naples, Italy

<sup>2</sup> Italian Space Agency, Via Del Politecnico, 00133 Rome, Italy

$R_{ci}$	Radius of the initial circular orbit, km
$\Omega$	Right ascension of ascending node, deg
$\dot{r}$	Regression rate, mm/s
$a$	Semi-major axis, km
$a_e$	Semi-major axis of elliptical orbit, km
$I_{sp}$	Specific impulse, s
$J_2$	Spherical harmonic coefficient of degree 2, km <sup>5</sup> /s <sup>2</sup>
$I_{tot}$	Total impulse, N s
$L_{tot}$	Total length, mm
$\nu$	True anomaly, deg
$\dot{M}$	Variation in time of mean anomaly, deg/s
$\dot{\Omega}$	Variation per unit time of the right ascension of ascending node, deg/s

## 1 Introduction

In recent years, the use of CubeSats has become increasingly popular due to their simplicity of construction, cost, and reduced production time compared to conventional satellites. These miniaturized satellites are well suited to formation flight for telecommunication and imaging purposes [1]. In this study, the formation flight of a 16U CubeSat constellation (RODiO [2–4], consisting of four micro-satellites) was analyzed with respect to a low earth orbit (LEO) satellite. The objective is to perform maneuvers to extend the virtual SAR antenna [5, 6]. In the following sections, the orbital maneuvers considered were described. The phasing maneuver is utilized to establish an along-track baseline, whereas the inclination change maneuver aims to generate a cross-track baseline.

To execute these maneuvers, a propulsion system capable of providing the right  $\Delta V$  and meeting the requirements of small size consistent with CubeSat dimensions, safety, re-ignition and throttle capabilities is needed. A Solid Rocket Motor could indeed generate a substantial thrust in a brief burn time, which would satisfy the mission requirement. However, it cannot be used for the maneuvers being studied due to the problem of re-ignition capability (once combustion is initiated in a Solid Rocket Motor, the system cannot be turned off and on again) as well as safety concerns (as fuel and oxidizer are always in contact, there is a possibility for spontaneous and unintended ignition). In addition, it is not possible to control the thrust value of a Solid Rocket Motor once the grain geometry is fixed and combustion is ignited. This is because the thrust profile is already defined and the flow rate exiting the nozzle cannot be modulated. With a Liquid Rocket Engine, the propulsion system satisfies controllability, re-ignition, and safety requirements because oxidizer and fuel are physically separated, which makes unintentional ignitions impossible [7]. However, the challenge with this type of rocket lies in its size and complexity,

which demands a separate tank for each propellant, two feed lines, and a complicated pressurization system. An electric propulsion system exhibits thrust values [7] that are insufficient for the studied application and would overload the satellite's Electrical Power Unit.

Nowadays, there are electric propulsion systems that turn out to be compact and have manageable power consumption even for CubeSat [8]. The high specific impulse allows them to operate for extended mission times, therefore, they turn out to be very useful to compensate all or part of the aerodynamic drag, so as to slow down the orbital decay. The thrust values exhibited are in the range of 300  $\mu\text{N}$  to 900  $\mu\text{N}$  which does not provide the ability to perform orbital maneuvers in rapid time. As will be seen below (in Sect. 3), for the total impulse required (on the order of hundreds of Newton seconds) with a typical electric thruster, ignition of the rocket would last for days. This deviates from the assumption of an impulsive burn and prevents the possibility of orbital maneuvers in a few orbital periods (such as the phasing maneuver, in depth discussed in Sect. 2). Another option is using monopropellant thrusters [9]. Due to their simplicity and small size, they can be safely installed on a CubeSat. However, the low specific impulse value, resulting in increased system volume, limits its effectiveness for the applications discussed in this paper. Several studies propose the use of cold-gas propulsion systems for CubeSats, primarily as actuators for attitude control systems [10, 11]. According to [10], these thrusters typically provide milli-Newton thrusts with low specific impulses, typically around 100 s [11]. Therefore, there is a need for volumes that are not compatible with the small size requirements of CubeSats.

Based on these factors, the decision was made to use a Hybrid Rocket Engine, which provides the necessary thrust values for maneuvering. Since the oxidizer is in liquid form, the fuel is in solid form, and they are stowed separately, the risk of unwanted ignitions is averted. Finally, the propulsion system provides a single feed line for the oxidizer, making it simpler than that of a Liquid Rocket Engine. In recent years, numerous studies have been performed on Hybrid Rocket Engines, evaluating their internal ballistics [12], assessing the performance of various oxidant-fuel pairs [13], and considering different thrust classes (200 N [14], 1 kN [15]). Based on the research group experience on larger-scale hybrid rockets, a 10 N thruster was designed, that is compatible with the dimensions of a CubeSat. Additionally, it should be noted that recent research has focused on the use of hybrid propulsion systems for CubeSats and other satellites [16, 17]. However, this research pertains to outer planet exploration missions and requires rocket designs on a different scale than the one discussed in this study, which focuses on reconfiguration maneuvers and a 10-N thrust scale.

Using GMAT (General Mission Analysis Tool) [18] an estimation of the maneuvers  $\Delta V$  budget was obtained. The

simulations validate the results obtained from Keplerian mechanics. On identifying the maneuvers' costs, a preliminary design of the Hybrid Rocket Engine for the CubeSat was carried out taking into account the results obtained by Mungiguerra et al. reported in [19], complying with the requirements for propulsion unit volume ( $< 1.5$  U) and mass ( $< 2$  kg).

## 2 Orbital Maneuvers Analysis

The study of orbital maneuvers is achievable through the application of Keplerian mechanics. In this study, it is assumed that the  $\Delta V$  application is impulsive, providing an instantaneous change in velocity, and therefore, neglecting the effects of burn finiteness. This assumption was made due to the inability to determine the thruster's burning time a priori.

The burning time can only be calculated after determining the necessary  $\Delta V$  to execute the maneuvers, given the satellite's mass and thruster's effective thrust. As the firing time obtained through subsequent paragraphs is significantly less than the characteristic times of the maneuvers, the assumption of instantaneous burning does not affect the results of the orbital maneuvers' analysis.

### 2.1 Satellite Characteristics and Assumptions for Orbital Maneuvers

The CubeSat RODiO constellation is composed of four satellites equipped with a receiving antenna, while the LEO satellite is equipped with a transmitting antenna. The LEO-satellite is moving on a quasi-circular Sun-Synchronous Orbit (eccentricity  $\approx 10^{-3}$ , inclination  $\approx 97^\circ$ ) at a mean altitude of  $\approx 400$  km (World Geodetic System-84), and RODiO cluster follows it on this orbit.

The following sections present methods for analyzing orbital maneuvers and results. Initially, the relative motion is studied considering the Hill reference frame discussed in [20], and under the assumptions of Keplerian mechanics reported in [21]. In this way, an initial estimate of the cost

of the maneuvers and the order of magnitude of the achievable along-track and cross-track baselines are obtained. Subsequently, simulations were performed with NASA *GMAT* software, with the following set-up:

- Gravitational harmonics up to order and degree 100 (EGM-96 model).
- Atmospheric drag (Jacchia-Roberts model, and CD value of 2.2 in compliance with [22]).
- Solar radiation pressure with a Solar radiation of  $1367 \text{ W/m}^2$ .
- Third body effects of Moon and Sun.

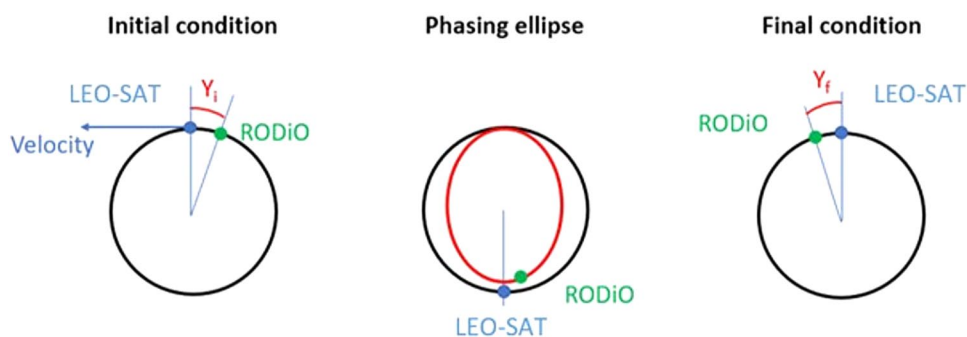
### 2.2 Phasing Maneuver

In this maneuver, the objective is to bring one of the satellites of the RODiO cluster, which follows the LEO-satellite in its orbit, from a distance in the range  $[-90 \text{ km}, -50 \text{ km}]$ , to a distance in the range  $[+50 \text{ km}, +90 \text{ km}]$ . In this way a multistatic SAR data collection with a triplet of acquisitions over the same area at three different observation angles is possible.

To this aim, a  $\Delta V$  in the direction opposite to the motion must be applied. In this way, the RODiO satellite reaches an elliptical orbit with an orbital period smaller than the period of the initial orbit and, after one orbit, the RODiO satellite reduces the along-track distance. After few orbits, the RODiO satellite reaches a new position beyond LEO-satellite and, at this point, a  $\Delta V$  in the motion direction must be applied to establish a constant along-track baseline. The steps of the maneuver just described are illustrated in the following Fig. 1. The challenging point of this mission is the need to apply two  $\Delta V$  but in opposite direction and evaluating the re-ignition capability of the propulsion system.

To study the relative motion between two satellites, the Hill reference frame defined in [20] was used, assuming that the LEO-satellite is the chief, while RODiO is the deputy. Combining the equations for the Hohmann transfer (under the assumptions of Keplerian mechanics and circular orbit), [21] reported in Eqs. 1, 2, 3, and 4, where:

Fig. 1 Steps of the phasing maneuver



- $V_{ci}$  is the orbital velocity of initial circular orbit,
- $\mu$  is the Earth's planetary gravitational constant,
- $R_{ci}$  is the radius of the initial circular orbit,
- $a_e$  is the semi-major axis of elliptical orbit,
- $\tau_{ci}$  is the period of the initial circular orbit,
- $\tau_e$  is the period of elliptical orbit,

it is possible to write Eq. 5, which provides an initial estimate of the along-track baseline variation per orbit ( $\Delta Y_{orbit}$ ).

$$V_{ci} = \sqrt{\frac{\mu}{R_{ci}}} \tag{1}$$

$$\tau_{ci} = 2\pi\sqrt{\frac{R_{ci}^3}{\mu}} \tag{2}$$

$$\Delta V = \sqrt{\mu\left(\frac{2}{R_{ci}} - \frac{1}{a_e}\right)} - \sqrt{\frac{\mu}{R_{ci}}} \tag{3}$$

$$\tau_e = 2\pi\sqrt{\frac{a_e^3}{\mu}} \tag{4}$$

$$\Delta Y_{orbit} = (\tau_{ci} - \tau_e)V_{ci} \tag{5}$$

In Fig. 2, the along-track baseline variation after one orbit respect to applicated  $\Delta V$  is shown.

In Table 1, different cases are presented, and a simulation of relative motion using GMAT, considering the set-up previously described, has been performed (results in Fig. 3).

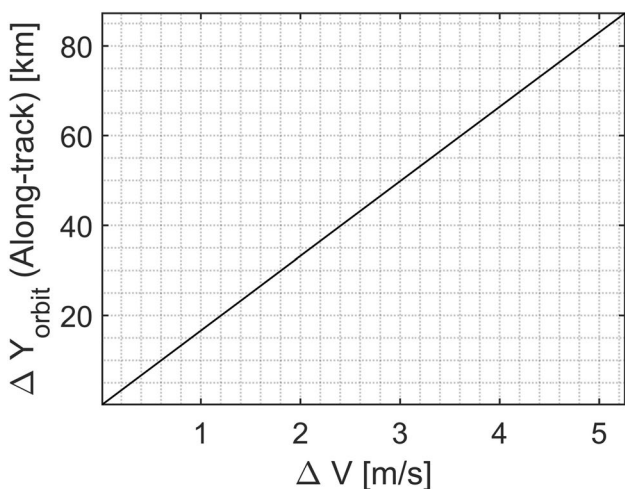


Fig. 2 Trend of along-track baseline variation per orbit with respect to  $\Delta V$  applied

Table 1 Possible phasing maneuvers in the along-track distance ranges considered for different  $\Delta V$

$\Delta V$ of single burn [m/s]	$Y_i$ [km]	$\Delta Y_{orbit}$ [km]	Number of orbits	$Y_f$ [km]
2.5	- 62.25	41.5	3	+ 62.25
3	- 75	50	3	+ 75

$Y_i$  is the initial distance between a RODiO satellite and the LEO-satellite,  $Y_f$  is the final distance

### 2.3 Inclination Change Maneuver

The purpose of this maneuver is to change the inclination of the orbit of a satellite of the RODiO constellation by applying a  $\Delta V$  normal to the orbital plane when the satellite arrives in the ascending node. In this way a relative drift of the nodes starts, and, after a certain time, a cross-track baseline is established. Applying an impulsive burn in the same direction but when the satellite reaches the descending node, the cross-track baseline remains constant. An advantage of this maneuver is that the direction of  $\Delta V$  does not change.

First, in the Keplerian mechanics assumptions (and considering circular orbit) it is possible to calculate the inclination variation of the orbit consequent to the application of an impulsive burn normal to the orbital plane. This maneuver is possible because the two orbits (the initial circular orbit and the one obtained by applying  $\Delta V$  in the normal direction) have two points in common: the ascending and the descending node. They are perfectly equivalent for a circular orbit. The situation reported in Fig. 4 is considered. It is possible to write the relation Eq. 6

$$\Delta V = 2V\sin\left(\frac{\Delta i}{2}\right) \tag{6}$$

where:

- $\Delta V$  is the velocity variation normal to orbital plane.
- $\Delta i$  is the inclination variation.
- $V$  is the orbit velocity.

From the relation Eq. 6, it is possible to observe that with  $\Delta V$ s in the order of magnitude of few meters per seconds, an inclination change of  $0.01^\circ$  can be obtained. In Fig. 5, the  $\Delta i$  obtained consequent to the application of an impulsive burn is shown.

Considering  $J_2$  effect, it is possible to calculate the cross-track baseline for  $\Delta V$  assigned. Under the assumption of quasi-circular LEO, it is possible to calculate the cross-track baseline from the equation of the relative motion [20]. It is possible to write the Eq. 7 from which the Eq. 8 is derived:

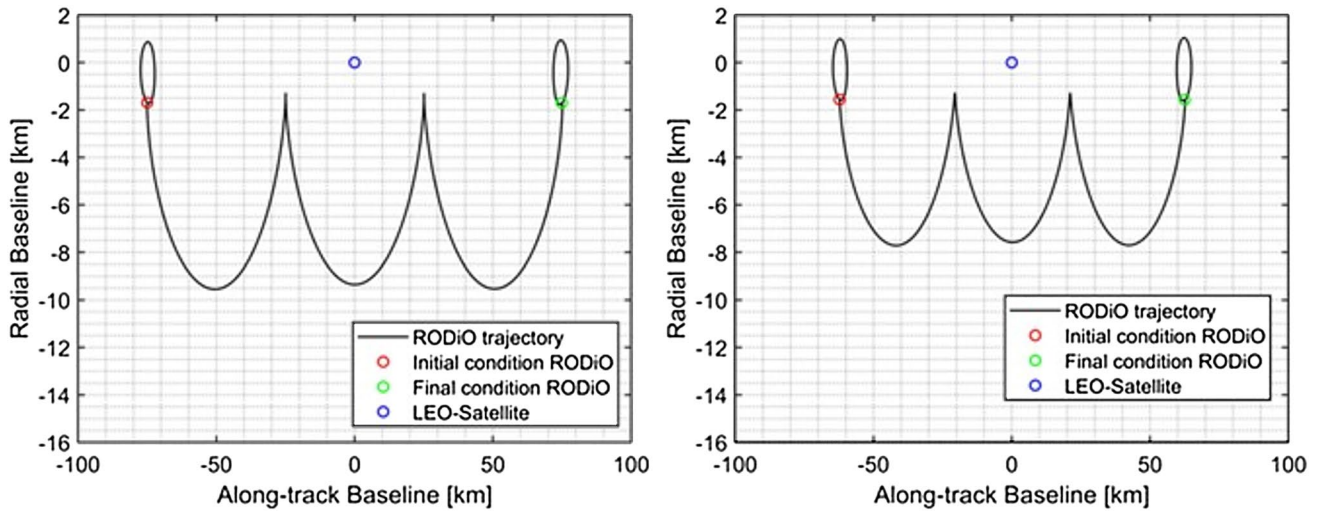


Fig. 3 RODiO trajectory in Hill reference frame with respect to LEO-Satellite (on the right, first case indicated in Table 1; on the left, second case indicated in Table 1)

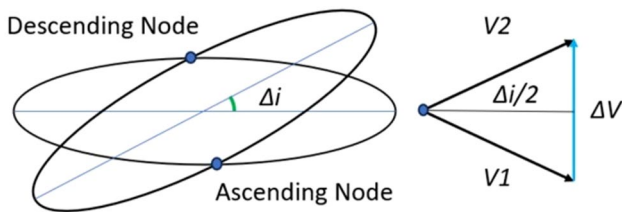


Fig. 4 Conceptual representation of change inclination maneuver: on the left the common points of initial and final orbit are indicated; on the right the mathematical construction for  $\Delta V$  calculation is reported

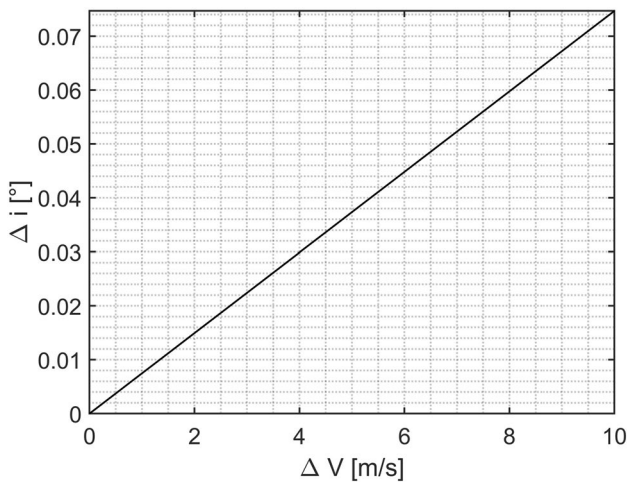


Fig. 5 Trend of  $\Delta i$  with respect to  $\Delta V$  applied

$$\dot{\Omega} = -\frac{3}{2}J_2\left(\frac{R_E}{p}\right)^2 \dot{M}\cos(i) \mathbf{i} \tag{7}$$

$$\Delta\dot{\Omega} = \frac{3}{2}J_2\left(\frac{R_E}{p}\right)^2 \dot{M}\sin(i)\Delta i \tag{8}$$

where:

- $\dot{\Omega}$  is the variation per unit time of the right ascension of ascending node.
- $J_2$  is the spherical harmonic coefficient of degree 2.
- $R_E$  is the Earth radius.
- $\dot{M}$  is the variation in time of mean anomaly.
- $p$  is the periapsis.
- $i$  is the orbital inclination.

Applying the impulsive burn allows for the calculation of  $\Delta i$ , and subsequently, the calculation of  $\Delta\dot{\Omega}$ . From the third of the following equations (Eq. 9), considering  $\delta i^2 \ll \delta\Omega^2$ , for a determined cross-track baseline, and knowing the semi-major axis, it is possible to calculate  $\Delta\Omega$ . From the ratio between  $\Delta\Omega/\Delta\dot{\Omega}$  it is possible to evaluate the time to obtain the desired cross-track baseline, using the simplified relation of equation Eq. 10:

$$\begin{bmatrix} x \\ y \\ z \end{bmatrix} \cong a \begin{bmatrix} \frac{\delta a}{a} - \delta e \cos(\nu) \\ 2\delta e \sin(\nu) + \delta\omega + \delta M_0 + \delta\Omega \cos i - \frac{3}{2}(\nu - \nu_0)\delta a \\ \sqrt{\delta i^2 + \sin^2(i)\delta\Omega^2} \cos(\omega + \nu - \phi) \end{bmatrix} \tag{9}$$

$$z_{\max} \approx a\delta\Omega \sin i \tag{10}$$

where  $\nu$  is the true anomaly, the subscript “0” stands for the initial conditions and the angle  $\phi$  corresponds to (Eq. 11)

$$\phi = \tan^{-1}\left(\frac{\delta i}{-\delta\Omega\sin i}\right) \quad (11)$$

In the following Fig. 6, the cross-track baseline obtained for different  $\Delta V$  and waiting time is shown.

In conclusion, the study of relative motion between two satellites of RODiO cluster has been analyzed using GMAT (RODiO-1 is the chief, RODiO-2 is the deputy). In Fig. 7, the results obtained by GMAT for a  $\Delta V=3$  m/s (that yields a  $\Delta i$  of 0.02 deg [21]) for each burn and a waiting time of 15 days are shown. The simulations confirm the results obtained from Keplerian mechanics.

## 2.4 Conclusions on Orbital Maneuvers Study

From numerical GMAT simulations, it is possible to conclude that the along-track baseline variations are possible to move one RODiO satellite from the original position to

a final position in few orbits, whereas cross-track baseline variations up to few kilometers are possible with maneuvers duration of the orders of few days. The maneuvers under consideration are intrinsically safe thanks to the appropriate selection of orbital parameters. Specifically, the RODiO satellite, which the  $\Delta V$ s are applied to, is in relative motion with respect to the LEO-satellite on a safety tube that eliminates any potential collision risks. If the RODiO CubeSat is brought into a forward position during the phasing maneuver and no additional station keeping is implemented (such as an electric propulsion system), the CubeSat could collide with the LEO-Satellite which is decaying faster. Due to the formation of a safety tube, as illustrated in Fig. 3, the LEO-Satellite can pass through it safely without the risk of colliding with the CubeSat RODiO. This issue is not a concern in the case of the inclination change maneuver, as the CubeSat RODiO assumes a new position outside of the initial orbital plane.

The prescribed  $\Delta V$  for hybrid propellant rocket sizing is 3 m/s per ignition, totaling 6 m/s. This value is preferred as it provides more comprehensive coverage in the phasing maneuver, spanning from  $[-90$  km;  $-50$  km] to  $[50$  km;  $+90$  km], compared to the less effective 2.5 m/s per ignition. Additionally, the inclination change maneuver creates a cross-track baseline of considerable interest (on the order of kilometers), in relatively short periods. Increasing the  $\Delta V$  would promote the development of a bigger cross-track baseline in a shorter period. However, it would result in the production of a cumbersome propulsion system.

Of the two maneuvers shown, the orbital inclination change maneuver proves to be the most relevant for SAR products. For stereoradargrammetric applications [6], acquiring data from different lines of sight is crucial. Therefore, because three out of the four satellites in the RODiO constellation share the same orbital plane as the LEO-Satellite, obtaining an acquisition point outside of this plane through an inclination change maneuver is more interesting than shifting in the same plane. Choosing this maneuver in future project stages for both increased safety, due to the

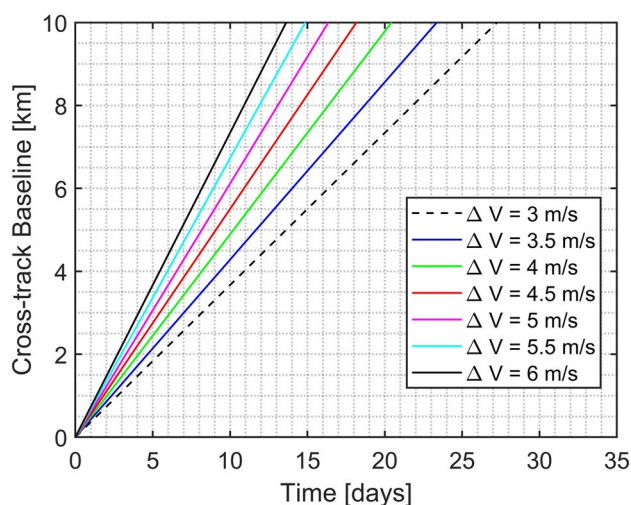
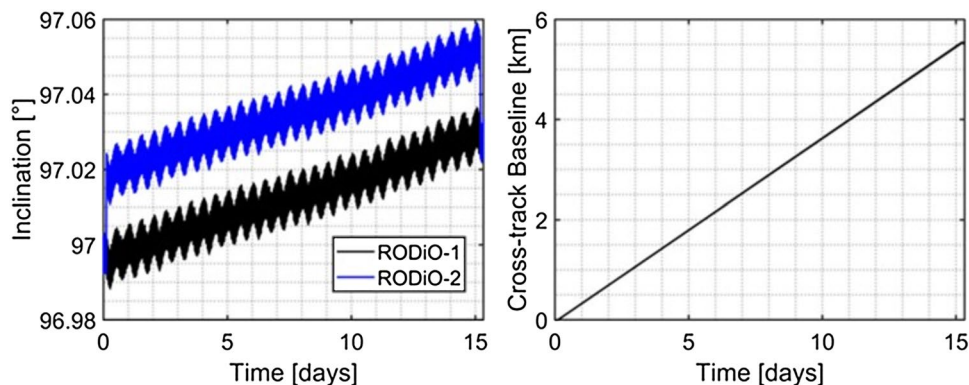


**Fig. 6** Trend of cross-track baseline with respect to the waiting time for applied  $\Delta V$

**Fig. 7** Trend of inclination (on the left) and trend of cross-track baseline (on the right) with respect to mission time for  $\Delta V=3$  m/s



elimination of collision risk resulting from the orbital plane change, and SAR product purposes would be advantageous.

### 3 Hybrid Rocket Engine Preliminary Design

This section focuses on the design of the hybrid rocket engine. In the following, the requirements and guiding assumptions for the sizing are presented which are derived from the experience of the UNINA DII [23]. The performance calculation involves performing a procedure [24], adapted to this study, that stops when the total impulse mission requirement is met. Lastly, a CAD model of the thrust chamber and a first estimate of the masses of the propulsion unit are presented.

#### 3.1 Requirements and Assumptions

From the analysis of orbital maneuvers, the mission objective (stated earlier) determines that the propulsion system must be capable of providing a total  $\Delta V$  of 6 m/s. In this pre-design, the total  $\Delta V$  should be amplified by 100% (total  $\Delta V$  with margin: 12 m/s) adhering to the guidelines laid out by ECSS [25]. From the study of orbital maneuvers and known characteristics of the satellite, the mission requirement on the total impulse is obtained with the simplified Eq. 12, valid with a good approximation in case of small propellant mass with respect to overall satellite mass [26], which is the case of this system. In Eq. 12,  $T$  is the thrust,  $t_b$  is the burning time,  $M$  is the mass of the satellite, and  $\Delta V$  is the change in velocity first determined.

$$I_{\text{tot}} = T t_b = \Delta V M \quad (12)$$

Taking into account the mass of the RODiO satellite (of 36 kg), the requirement on  $\Delta V$  results in a requirement on the total impulse of 432 N s. For this preliminary sizing of the thrust chamber, to reduce the loads on the tanks and fluidic lines, the following constraints were selected:

- $10 < P_c < 15$  bar
- $T = 10 \pm 5$  N

The requirement of the combustion chamber pressure derives from a compromise between the need for a good HTP (high test peroxide) decomposition efficiency (increased at a relatively high pressure [9]) and disadvantageous effect of increasing storage pressure on the HTP tank sizing.

Moreover, although this is not a stringent requirement, to avoid undesirable fluid-dynamic configurations, it is preferred to have, for the whole firing duration, a ratio between grain length and port diameter higher than 1. The thrust and pressure requirements have a significant impact on the

size of the thrust chamber. A thrust range of  $10 \pm 5$  N was selected to ensure the engine's feasibility on a CubeSat-compatible scale, while avoiding excessive pressure in the chamber to prevent potential thermal and mechanical stresses that could be critical due to the thruster's small size. The earlier mentioned maneuvers are based on the impulsive burn hypothesis. For the hypothesis to be valid, a thrust with a duration that is not excessive is required. If the thrust is in the milli-Newton range, the burn would last for days. On the other hand, if the thrust is too high, around 100 N, the inertial loads on the satellite structure may be excessive, and the attitude control system may not be able to counteract the torques induced by potential thrust axis misalignments with respect to platform center of mass. From these considerations, the thrust range  $10 \pm 5$  N was chosen.

A mixture with hydrogen peroxide as oxidant (91wt%) and HDPE (high-density polyethylene) as fuel grain is selected to evaluate the performance of the Hybrid Rocket Engine.

#### 3.2 Calculation Procedure

To perform the calculation, it is required to establish the initial grain geometry in terms of length and port diameter, as well as the oxidant mass flow rate (values for these quantities are given in Sect. 3.3). The initial oxidant mass flux can be determined based on the oxidant mass flow rate and the initial port diameter. In first approximation, the regression rate for a hybrid rocket motor is related to oxidizer mass flux (Eq. 13):

$$\dot{r} = a(G_{\text{ox}})^n \quad (13)$$

where “ $a$ ” and “ $n$ ” are experimental coefficients which change for each couple of propellants. To accurately calculate performance [24], it is necessary to know the fuel grain geometry (initial port diameter and length), fuel density, burn time, expansion ratio and nozzle throat diameter, oxidant flow rate, and the regression rate law.

Integrating Eq. 13 in time, the instantaneous port diameter was calculated. Then, considering the prescribed oxidizer mass flow rate, the corresponding mass flux and regression rate was estimated. Then, the fuel mass flow rate was calculated as (Eq. 14):

$$\dot{m}_f(t) = \rho_f \pi D(t) L \dot{r}(t) \quad (14)$$

where  $\rho_f$  is the solid fuel density,  $L$  is the length of the grain. In addition, the oxidant to fuel ratio is calculated as (Eq. 15):

$$\text{OF} = \frac{\dot{m}_{\text{ox}}}{\dot{m}_f} \quad (15)$$

Once all these quantities are known, the rocket performance can be evaluated using software as CEA (chemical

equilibrium analysis) [27]. Since the chamber pressure is unknown, the iterative procedure given in [24] is applied until the pressure value that satisfies the mass balance is found.

For the calculation of the performance by [24], it is necessary to know the burning time, which is a priori unknown. Thus, a time step of 0.5 s can be set, for which the performance of the thruster is calculated, and when the desired total impulse is reached, the iterations are stopped, obtaining the burn time and the final grain diameter. The logical progression is shown in Fig. 8.

### 3.3 Performance Analysis and Results

A first assumption on the grain, pre-chamber, post-chamber and nozzle converging part length was based on the previous experience acquired by the authors in previous research projects [23] in order to guarantee acceptable residence time and flow field. An initial port diameter of the grain equal to 10 mm was selected. The reference quantities for the analysis are reported in Table 2. The sum of these contributions gives the total length, whose formula is expressed by Eq. 16.

The nozzle throat diameter was chosen after a few iterations, based on the chamber pressure value obtained. With the value chosen and shown in Table 2, a chamber pressure

**Table 2** Reference quantities for the simulations

$L_{pre}$ [mm]	$L_{grain}$ [mm]	$L_{conv}$ [mm]	$L_{post}$ [mm]	$D_t$ [mm]	$A_e/A_t$
10	35	10	10	2.6	20

in the range given in the requirements was obtained. The divergent part length was evaluated assuming a conical shape with 15 deg divergence angle. Optimization of the obtained values may be performed considering bell-shaped nozzles.

$$L_{tot} = L_{pre} + L_{grain} + L_{post} + L_{conv} + L_{div} \quad (16)$$

All the simulations have been performed with a combustion efficiency equal to 95%, a reasonable value according to the experiments that have already been performed. Nozzle efficiency is also set to 95%, giving a global efficiency of roughly 90%.

To obtain the regression law coefficients for the Eq. 13, the ballistic reconstruction technique reported in [28–30], was used. Ballistic reconstruction techniques have been introduced to reproduce the temporal trend of the regression rate during the burning time and to increase the number of experimental tests used for the development of accurate and reliable regression laws. Based on the experimental data regarding the mixture  $H_2O_2$ -HDPE [19], preliminary results of ballistic reconstruction technique on this scale of engine was used to obtain the coefficients “a” and “n”.

Table 3 shows the performance of the Hybrid Rocket Engine, calculated for three different oxidant mass flow rates. The Hydrogen Peroxide total mass required is 128 g. In all three scenarios analyzed, the mission objective has been accomplished, and the progressions of the main quantities over time are shown from Figs. 9, 10, 11, 12, 13, 14.

The data suggest that the thrust remains approximately constant over time, while the specific impulse increases with time for all three oxidant flow rates, reaching a value

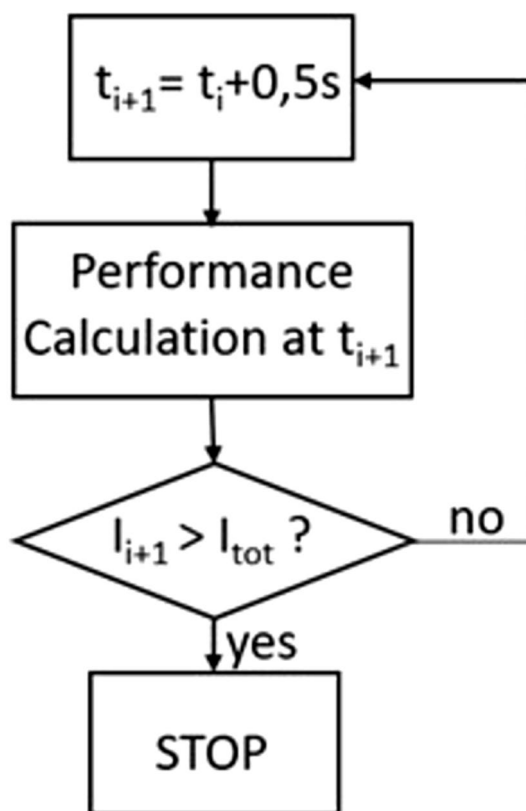


**Fig. 8** Conceptual scheme of the simulation

**Table 3** Mean values of the main quantities for the different oxidant mass flow rates under consideration

$\dot{m}_{ox}$	3 g/s	3.5 g/s	4 g/s
$I_{sp}$ [s]	288.1	289.8	291.3
Thrust [N]	10.2	11.9	13.6
$O/F$	5.01	5.19	5.35
$P_c$ [bar]	10.6	12.4	14.2
$D_p$ [mm]	24.3	23.8	23.6
$\dot{r}$ [mm/s]	0.27	0.31	0.35
$\dot{m}_{fuel}$ [g/s]	0.61	0.68	0.76
$G_{ox}$ [kg/m <sup>2</sup> s]	8.57	10.26	11.98
$t_b$ [s]	42.5	36.5	32



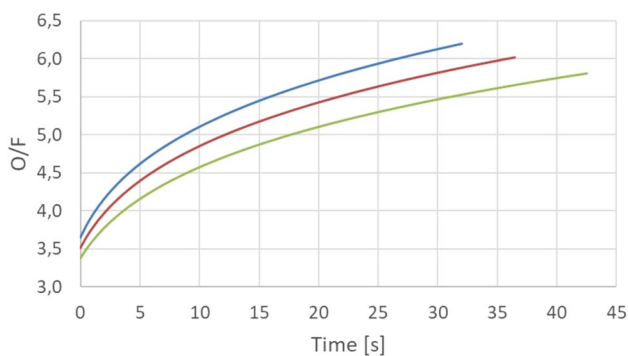


**Fig. 9** O/F in time evolution of  $H_2O_2$ -HDPE mixture for oxidant mass flow rate 3 g/s (in green), 3.5 g/s (in red) and 4 g/s (in blue)

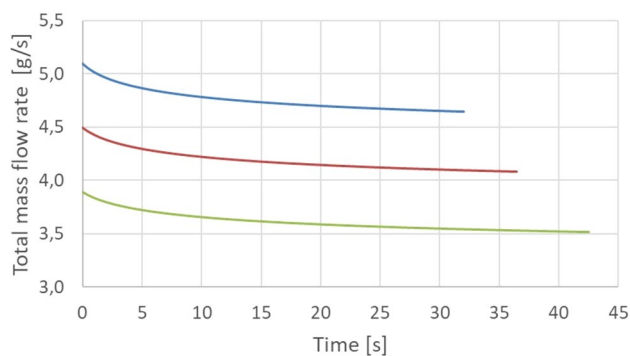


**Fig. 12** Total mass flow rate in time evolution of  $H_2O_2$ -HDPE mixture for oxidant mass flow rate 3 g/s (in green), 3.5 g/s (in red) and 4 g/s (in blue)

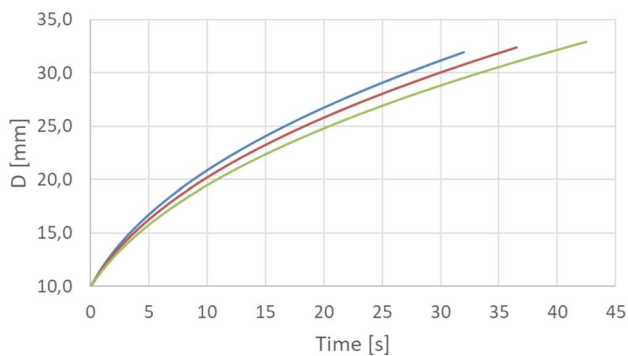


**Fig. 10** Grain port diameter in time evolution of  $H_2O_2$ -HDPE mixture for oxidant mass flow rate 3 g/s (in green), 3.5 g/s (in red) and 4 g/s (in blue)

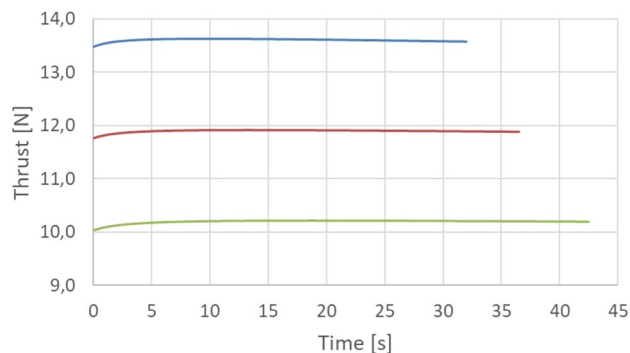


**Fig. 13** Thrust in time evolution of  $H_2O_2$ -HDPE mixture for oxidant mass flow rate 3 g/s (in green), 3.5 g/s (in red) and 4 g/s (in blue)

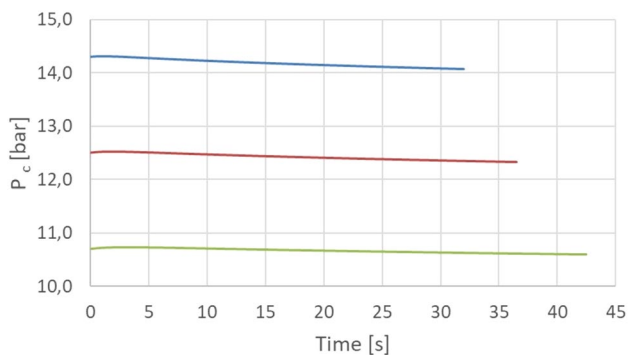


**Fig. 11** Chamber pressure in time evolution of  $H_2O_2$ -HDPE mixture for oxidant mass flow rate 3 g/s (in green), 3.5 g/s (in red) and 4 g/s (in blue)

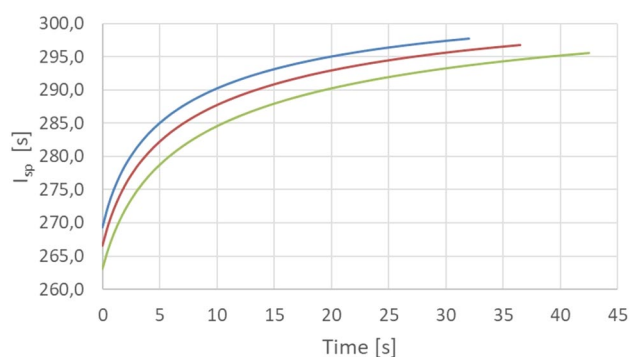


**Fig. 14**  $I_{sp}$  in time evolution of  $H_2O_2$ -HDPE mixture for oxidant mass flow rate 3 g/s (in green), 3.5 g/s (in red) and 4 g/s (in blue)

between 295–300 s. It is important to note the possibility of the rocket thrust axis not being barycentric, resulting in a moment that the AOCS (Attitude and Orbit Control System) must balance. For this reason, it is recommended to eliminate the option of implementing a flow rate of 4 g/s, which generates the highest thrust value but would cause

more significant moments that can potentially affect the AOCS. Conversely, using low-thrust values increases the burning time, prolonging thermal flux action and elevating the risk of thermal failure. A suitable compromise between burning time and thrust value results in selecting a solution where the oxidizer flow rate is 3.5 g/s.

Additionally, it is noteworthy that the utilization of hydrogen peroxide enables preheating of the catalyst chamber without the requirement of igniters. A pulsed sequence, such as the one described in [31], can effectively achieve adequate preheating, which is crucial for ensuring the decomposition of  $\text{H}_2\text{O}_2$ .

The quantity of hydrogen peroxide utilized for preheating is factored into the margin of the  $\Delta V$ . The conducted sizing is useful for determining the limiting dimensions of the thrust chamber and obtaining an initial idea about the main quantities of the hybrid rocket engine.

Variations may occur due to the two ignitions that need to be performed, each of which is affected by an ignition delay and a shutdown transient. Tests conducted on this scale of engines [19] show that the ignition and shutdown transients last for tenths of seconds, and the propellant consumption due to these phases is easily accounted for by the 100% margin on the mission requirement considered. From [32], it is possible to see the ignition delay for a hybrid rocket engine based on 95 wt.%  $\text{H}_2\text{O}_2$ , but on a larger scale (250 N).

It is noted that the ignition delay is between 0.3 and 1 s, which confirms what is reported in the thrust profile in [19], and since relative motion always develops over times on the order of a few orbital periods, any thrust present during these transients (which is considerably less than the steady-state thrust value) may not make appreciable changes to the maneuvers. If the mission profile deviates from the nominal, the strong controllability of a hybrid engine can always be exploited. For instance, if there is a significant ignition delay in which a certain proportion of the expected total impulse is reached, it is always possible to reduce the burn time to guarantee the total impulse calculated during the design phase. Subsequent developments will involve breadboarding

activities designed to accurately evaluate the on/off transients on this scale of rocket.

### 3.4 Preliminary CAD Configurations

From the performance analysis, it is possible to preliminarily size the propulsion system, in particular the thrust chamber, which will include a case containing the fuel grain and nozzle. Figure 15 shows a sectional view of the thrust chamber obtained for an oxidant mass flow rate of 3.5 g/s, with the maximum overall dimensions indicated, from which it is possible to observe a pre-combustion chamber (upstream of fuel grain), a post-combustion chamber (downstream of the fuel grain) consisting of a cylindrical section and the converging nozzle section. The pre- and post-chamber lengths shall be better defined by a more accurate study of the rocket's internal thermo-fluid dynamics.

For the various components of the thrust chamber, the materials shown in Table 4 were selected, and the masses estimated. Since the dimensions of the thrust chamber are considerably smaller than the imposed limits (1.5 U, 15 cm in height  $\times$  10 cm in length  $\times$  10 cm in width), it is reasonable to assume that there is sufficient space for the feed line,

**Table 4** Summary of thrust chamber masses by component

Part	Material	Mass [g]
Grain	HDPE	26
Case	Stainless steel 316	146
Flange	Stainless steel 316	28
Nozzle	Graphite	42
Total		242

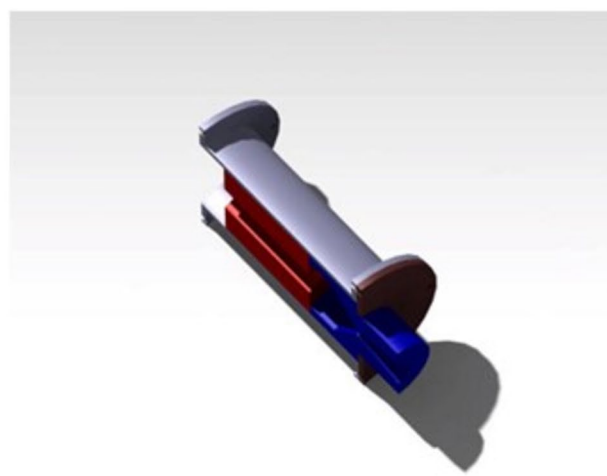
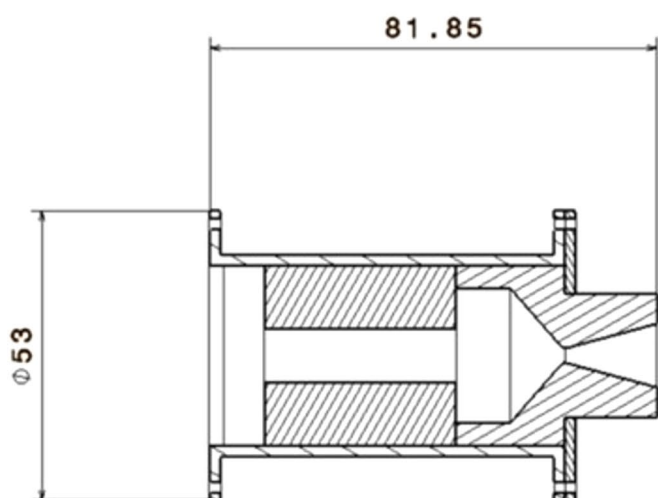


**Fig. 15** CAD model section of thrust chamber (dimensions in mm). In blue the conical nozzle, in red the fuel grain, in gray the external case, in brown a closing flange (wall thickness flange and case: 2 mm)

tanks, and catalytic chamber. With an appropriate choice of materials, the total mass requirement ( $< 2$  kg) is also satisfied.

## 4 Concluding Remarks

In this work, a study was carried out for mission analysis and preliminary design of a hybrid rocket engine aimed at performing formation reconfiguration of a Cubesat cluster (RODiO), working as passive receiver of the SAR signal of a LEO satellite. Starting from considerations on Keplerian mechanics, maneuvering costs (in terms of  $\Delta V$ ) and achievable along-track and cross-track baselines have been calculated. With a total  $\Delta V$  of 6 m/s, it is feasible to achieve an along-track baseline in the range of tens of kilometers with a waiting time of a few orbits. Conversely, achieving a cross-track baseline in the order of a few kilometers would take a few days. Furthermore, GMAT was used to accurately simulate orbital maneuvers and validate the findings from Keplerian mechanics.

The application of the  $\Delta V$  identified earlier allows the execution of orbital maneuvers useful for changing the configuration of the RODiO constellation for the purpose of improving SAR antenna performance, both in-plane (phasing maneuver) and out-of-plane (inclination change maneuver). It is recommended to prefer the inclination change maneuver over the phasing maneuver for collision risk mitigation and SAR product utility. The preliminary performance calculation (for a total  $\Delta V$  of 12 m/s with margin in compliance with ECSS regulation) provides an initial output on the design of the thrust chamber and the average values of the quantities involved. The mission requirement is met for the three configurations analyzed, which differ only in the oxidizer flow rate. Trend analysis of principal quantities indicates that a thrust chamber experiences higher pressures for shorter durations under a 4 g/s flow rate. Conversely, the chamber operates at lower pressures for more extended periods with a 3 g/s flow rate. As previously noted, it is optimal for the thrust to be minimized to allow for minor moments caused by the misalignment of the thrust axis from the center of gravity to be easily compensated by the AOCS system. On the other hand, prolonged burning time can result in thermal and structural issues. In particular, the thermal aspect appears to be crucial due to the rocket's small size. Conducting meticulous analyses to assess the thermal fluxes affecting the thrust chamber during the operating time for all three alternatives will enable the determination of the optimum solution. At this time, a suitable compromise would be selecting an oxidant mass flow rate value of 3.5 g/s.

Two configurations are possible for the layout of the elements of the propulsion unit: a first configuration in which the engine is developed in height, with the thrust chamber

placed in succession to the tanks; a second configuration in which it is planned to place the tanks around the thrust chamber. Given the 1.5 U dimensional constraints (15 cm in height  $\times$  10 cm in length  $\times$  10 cm in width), and the minimal space occupied in the radial direction, it is preferable to optimize available space by locating the other elements of the propulsion unit around the thrust chamber (i.e., using toroidal tanks). Indifferently from the two configurations, it is reasonable to conclude that the propulsion unit meets the required mass ( $< 2$  kg) and size ( $< 1.5$  U) constraints. Future developments could include a detailed design of the other main subsystems, numerical analysis of fluid dynamic, thermal and structural aspects, and the possibility of developing breadboards for ground testing of the propulsion unit.

**Acknowledgements** This activity is funded by the Italian Space Agency in the framework of RODiO project (ASI contract 2022-28-I.0, project number F63C22000720005).

**Funding** Open access funding provided by Università degli Studi di Napoli Federico II within the CRUI-CARE Agreement. Agenzia Spaziale Italiana, 2022-28-I.0.

**Data availability** The datasets generated and/or analysed during current study are available from the corresponding author on reasonable request.

## Declarations

**Conflict of Interest** On behalf of all authors, the corresponding author states that there is no conflict of interest.

**Open Access** This article is licensed under a Creative Commons Attribution 4.0 International License, which permits use, sharing, adaptation, distribution and reproduction in any medium or format, as long as you give appropriate credit to the original author(s) and the source, provide a link to the Creative Commons licence, and indicate if changes were made. The images or other third party material in this article are included in the article's Creative Commons licence, unless indicated otherwise in a credit line to the material. If material is not included in the article's Creative Commons licence and your intended use is not permitted by statutory regulation or exceeds the permitted use, you will need to obtain permission directly from the copyright holder. To view a copy of this licence, visit <http://creativecommons.org/licenses/by/4.0/>.

## References

1. IAA, Study group on cost effective earth observation missions, IAA Position Paper on Cost effective Earth Observation Missions, 2004.
2. Renga, A., et al.: Design considerations and performance analysis for RODiO distributed SAR mission. *Acta Astronaut.* **210**, 474–482 (2023)
3. Leccese, G., et al.: Overview and roadmap of Italian Space Agency activities in the micro- and nano-satellite domain, 73rd IAC, Paris, France, 2022, 18–22 September.
4. Renga, A., et al.: Beamforming and multi-platform image synthesis for RODiO distributed SAR, 73rd IAC, Paris, France, 2022, 18–22 September.

5. Moccia, A., et al.: Spaceborne bistatic synthetic aperture radar for remote sensing applications. *Int J Rem Sens.* **21**(18), 3395–3414 (2010). <https://doi.org/10.1080/014311600750037453>
6. Renga, A., et al.: Performance of stereoradargrammetric methods applied to spaceborne monostatic–bistatic synthetic aperture radar. *IEEE Trans Geosci Rem Sens* (2009). <https://doi.org/10.1109/TGRS.2008.2003184>
7. Sutton, G., Biblarz, O.: Rocket propulsion elements, 7th (2001)
8. Manente, M., et al.: REGULUS: A propulsion platform to boost small satellite missions. *Acta Astronaut.* **157**, 241–249 (2019)
9. Cassese, S., et al.: Preliminary design and study of 5N HTP monopropellant thruster for small satellites. *Acta Astronaut.* **202**, 94–103 (2023)
10. Stevenson, T., et al.: Design and testing of a cold gas thruster for an interplanetary CubeSat Mission. *JoSS.* **4**(2), 371–386 (2015)
11. Lemmer, K.: Propulsion for CubeSats. *Acta Astronaut.* **134**, 231–243 (2017)
12. Di Martino, G.D., et al.: Transient computational thermofluid-dynamic simulation of hybrid rocket internal ballistics. *J. Propul. PowerPropul Power* (2017). <https://doi.org/10.2514/1.B36425>
13. Whitmore, S.A., et al.: Comparing hydroxyl terminated polybutadiene and acrylonitrile butadiene styrene as hybrid rocket fuels. *J. Propul. PowerPropul Power* (2013). <https://doi.org/10.2514/1.B34382>
14. Cardillo, D., et al.: Experimental firing test campaign and nozzle heat transfer reconstruction in a 200 N hybrid rocket engine with different paraffin-based fuel grain lengths. *Aerospace* **10**(6), 546 (2023). <https://doi.org/10.3390/aerospace10060546>
15. D. Cardillo et al. Testing 1kN paraffin-based hybrid rocket engine, 8th European Conference for Aeronautics and Space Sciences (EUCASS). <https://doi.org/10.13009/EUCASS2019-541>
16. Jens, E. T. et al.: Design of interplanetary hybrid cubesat and smallsat propulsion systems. Joint Propulsion Conference, July 9–11, 2018, Cincinnati, Ohio.
17. Jens, E.T., et al.: Hybrid rocket propulsion systems for outer planet exploration missions. *Acta Astronaut.* **128**, 119–130 (2016)
18. NASA, General Mission Analysis Tool (GMAT), user guide. <https://gmat.sourceforge.net/docs/nightly/html/index.html>
19. Mungiguerra, S. et al.: Experimental and numerical assessment of regression rate and propulsive performance of 10N-class hybrid rockets for nanosatellite maneuvering. 74th International Astronautical Congress (IAC), Baku, Azerbaijan, 2–6 October 2023.
20. D’Errico, M. (ed.): Distributed space missions for earth system monitoring, pp. 125–162. Space Technology Library, Springer Science Business Media, New York (2013)
21. Vallado, D. A.: Fundamentals of astrodynamics and applications. Space Technology Library, Springer Dordrecht, 2 edn, pp. 317–422.
22. Loth, E., et al.: Supersonic and hypersonic drag coefficients for a sphere. *AIAA J.* (2021). <https://doi.org/10.2514/1.J060153>
23. Grassi, M. et al.: FORCE: a formation flying SAR based on cube-Sat assemblies. 73rd International Astronautical Congress (IAC), Paris, France, 18–22 September 2022, IAC-22-B4.7.9.
24. Mungiguerra, S., et al.: Characterization of novel ceramic composites for rocket nozzles in high-temperature harsh environments. *Int. J. Heat Mass Transf.* **163**, 120492 (2020)
25. Walker, R.: System margin policy for ESA IOD CubeSat Projects, ESA TEC-SY/77/2016/POL/RW, Issue 1 Rev. 1 (2021).
26. Burton, R. L. et al.: Development of the MCD thruster for nanosat propulsion, JANNAF Conf., Colorado Springs, CO, Paper 1387 (2010).
27. Gordon, S. et al.: Computer program of complex chemical equilibrium compositions and applications. NASA Reference Publication, 1994 1311.
28. Gallo, G., et al.: New entrainment model for modelling the regression rate in hybrid rocket engines. *J. Propuls. Power.* **37**, 893–909 (2021). <https://doi.org/10.2514/1.B38333>
29. Gallo, G., et al.: Regression rate model assessed by ballistic reconstruction technique in hybrid rocket engines burning liquefying fuels. *Aerosp. Sci. Technol.* **127**, 107712 (2022). <https://doi.org/10.1016/j.ast.2022.107712>
30. Saito, Y. et al.: The accuracy of reconstruction techniques for determining hybrid rocket fuel regression rate. In: 2018 Jt. Propuls. Conf., American Institute of Aeronautics and Astronautics, Reston, Virginia. <https://doi.org/10.2514/6.2018-4923>. (2018)
31. Cassese, S. et al.: Experimental characterization of an impulsive hydrogen peroxide-based rocket for fine orbit control. 74th International Astronautical Congress (IAC), Baku, Azerbaijan, 2–6 October 2023. Copyright ©2023 by the International Astronautical Federation (IAF).
32. Kang, S. et al.: Design and performance evaluation of hybrid rocket using 95 wt.% H<sub>2</sub>O<sub>2</sub>. Propulsion and Energy Forum. 52nd AIAA/SAE/ASEE Joint Propulsion Conference, July 25–27, 2016, Salt Lake City, UT.

**Publisher's Note** Springer Nature remains neutral with regard to jurisdictional claims in published maps and institutional affiliations.